Expression and Binding of SARS-CoV-2 Variant of Concern Spike Proteins

Master thesis

by

Mirte Linthorst

Student number	5753961
Date	October 2020 – January 2022
Examiner	Dr. R.P. de Vries
Daily supervisor	Dr. K.M. Bouwman
Second Reviewer	Dr. Ing. T. Wennekes
Research group	Chemical Biology and Drug Discovery Utrecht Institute for Pharmaceutical Sciences Bijvoet Centre for Biomolecular Research

Utrecht University

Table of content

Layman’s abstract

The Severe Acute Respiratory syndrome coronavirus 2 (SARS-CoV-2) is a virus that emerged at the end of 2019 in China and caused a worldwide pandemic. It is one of the seven known human coronaviruses. The disease that is caused by the SARS-CoV-2 virus is called coronavirus disease 2019 (Covid-19). Up to now, there are more than 187 million reported cases of COVID-19 and over 4 million reported deaths. To terminate or prevent outbreaks, vaccination campaigns are introduced worldwide. However, the ability of the virus to adapt itself, makes it harder for the human body to correctly recognize the virus when it enters the body.

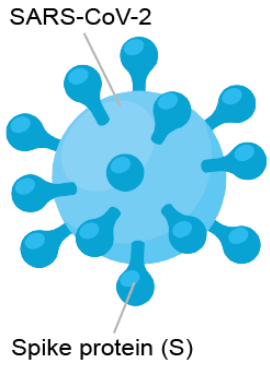

One of the regions of the coronavirus that adapts itself over time due to environmental and immune status, is the so-called spike protein. This is called drift and can lead to a reduced recognition by the immune system. It can also lead to differences in transmissibility, disease outcomes or host tropism. Since the beginning of the coronavirus pandemic, several adapted forms of the virus that have gained those concerning abilities, are designated as ‘variants of concern’ (VOC). A better insight into the spike protein variants of SARS-CoV-2 can help us to develop better drugs and vaccines. Therefore, this study investigated the ability of four variant of concern spike proteins to bind to cells and animal lung tissues.

In this research, an increased binding ability for two of the four variants of concern was observed. A new binding site in the spike protein of another VOC was discovered. Lastly, a host range extension to mice was confirmed for all four VOCs.

Although further research is required to confirm and extend these observations, this study provides an indication for new binding properties, which can in the future help us to develop new and better therapeutics against Covid-19.

Expression and Binding of SARS-CoV-2 Variant of Concern Spike Proteins

ABSTRACT

SARS-CoV-2 virus is one of the seven known human coronaviruses. At the end of 2019, this virus emerged in China and caused a worldwide pandemic. Since the beginning of the current coronavirus pandemic, the initial spike protein of SARS-CoV-2 has undergone several adaptive mutations in its gene, leading to new variants, coined as variants of concern (VOC). In this study, the receptor binding properties of the N-terminal (NTD) and C-terminal domain (CTD) of P.1, B.1.1.7, B.1.351 and B.1.351 R246I VOCs to cultured VERO-E6 cells and paraffin-embedded lung tissues of several animal models were investigated and compared to wildtype SARS-CoV-2. The obtained data provides grounds for increased binding properties of P.1-CTD and B.1.1.7-CTD, a newly introduced binding site in B.1.351-NTD as well as for B.1.351 R246I-NTD and a host range extension to mice for all four variants.

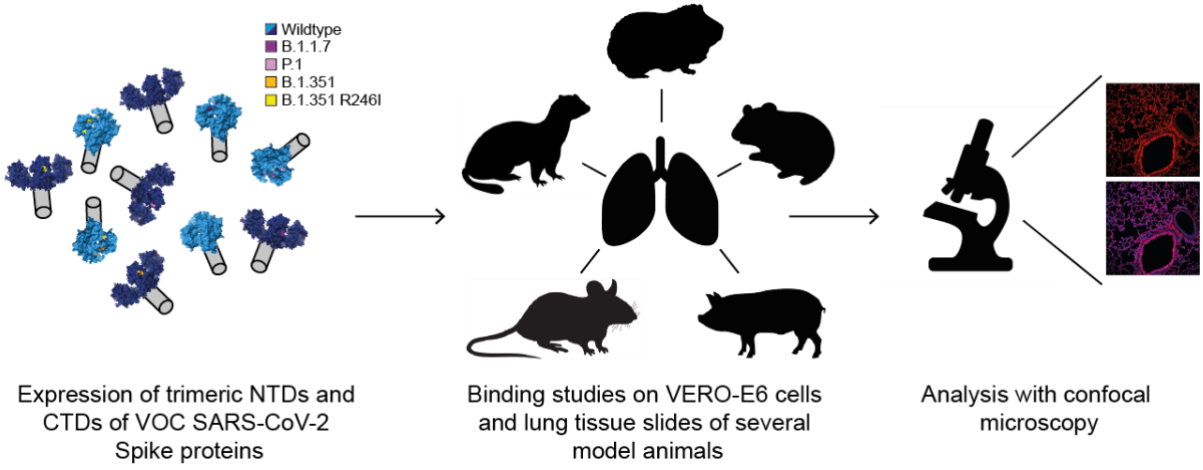

INTRODUCTION

Coronaviruses are positive-sensed single stranded RNA viruses, that are known to infect animals (mammals and avian species) as well as humans[1]. Coronaviruses are part of the *Coronaviridae* family, which is further classified into two subfamilies, the *Coronavirinae* and *Torovirinae*. The *Coronavirinea* subfamily consists of four genera: alpha- beta-, gamma- and delta. Human coronaviruses (HCoVs) all belong to either the alpha- or beta genus and are responsible for a range of acute and chronic diseases in humans[2]. Usually, infection with coronaviruses cause the common cold in humans. However, in some cases they can cause severe pneumonia, as well as enteric and neurological diseases, making it, especially for people with an impaired immune system, a lethal disease[1,3,4].

SARS-CoV-2, a new human coronavirus

To date, there are seven known human coronaviruses. 229E and NL63 belong to the alpha coronaviruses[5,6]. OC43, HKU1, MERS-CoV, SARS-CoV-1 and the recently emerged SARS-CoV-2 (severe acute respiratory syndrome coronavirus 2) are part of the beta coronavirus genus[7–11]. At the end of 2019, SARS-CoV-2 emerged in China[12,13]. Since then, it has caused a worldwide outbreak of the coronavirus disease 2019 (COVID-19). Up to now, there are more than 187 million reported cases of COVID-19 and over 4 million reported deaths[14]. To terminate or prevent outbreaks, vaccination campaigns are introduced worldwide. However, the ability of the virus to mutate, causes great challenges for the immune system to develop a

robust immunity which is still sufficient to react against new subtypes of the virus, leading to a constant threat for new major outbreaks[15,16].

One of the regions in the genome of SARS-CoV-2 that is prone to mutations, is the gene encoding for the spike protein (S protein, figure 1A-C). SARS-CoV-2 enters the cell by binding of the S protein to the Angiotensin-converting enzyme 2 (ACE2). The transmembrane protease serine 2 (TMPRSS2) on the host cell membrane is also needed for entry, since it plays a key role in priming the S protein[17]. The Spike is a homotrimer where each S protein consists of a S1 and S2 domain. The S1 domain is responsible for the binding of ACE2 and the S2 domain for the fusion of viral and host-cell membranes[18]. The S1 subunit can be further divided in the N-terminal domain (NTD) and the C-terminal domain (CTD). The SARS-CoV-2 S1-spike protein CTD contains the site that binds to ACE2[19]. However, there are also HCoVs that carry a binding site in the S1-spike protein NTD, such as OC43, HKU1 and MERS-CoV[20–23]. Since the beginning of the current coronavirus pandemic, the initial S protein of SARS-CoV-2, also known as the wildtype (wt), has undergone several adaptive mutations in its gene[24,25]. Although most mutations do not lead to amino acid mutations that change the properties of the virus, some can. Therefore, additional research to newly introduced viral strains is necessary.

SARS-CoV-2 variants of concern

If a new viral strain meets several requirements, it is classified as a variant of interest (VOI) or a variant of concern (VOC) by the World Health Organization (WHO)[26], where the requirements for a VOI are noted as:

- Presence of genetic changes that are predicted or known to affect virus characteristics such as transmissibility, disease severity, immune escape, diagnostic or therapeutic escape; AND
- Identified to cause significant community transmission or multiple COVID-19 clusters, in multiple countries with increasing relative prevalence alongside increasing number of cases over time, or other apparent epidemiological impacts to suggest an emerging risk to global public health.

When a variant fits the requirements of a VOI and in addition meets one of the following characteristics, it is classified as a VOC:

- Increase in transmissibility or detrimental change in COVID-19 epidemiology; OR
- Increase in virulence or change in clinical disease presentation; OR
- Decrease in effectiveness of public health and social measures or available diagnostics, vaccines, therapeutics.

Up to now, there are four lineages that are designated as a VOC[26,27] of which the NTDs and CTDs of three of them are studied here (figure 1D). B.1.1.7, also known as the alpha variant, was first identified in the United Kingdom in September 2020. The variant defining mutations positioned in the NTD are H69del, V70del and Y144del, and in the CTD, it contains a N501Y substitution[28,29]. Especially the N501Y substitution is considered to have an impact on the increased transmission that is seen for B.1.1.7, since this amino acid mutation causes an enhanced binding affinity to ACE2[30,31]. The mutant used in this report contains all the described mutations. B.1.351, the beta variant, which was identified in South Africa in May 2020, contains a L18F, D80A, D215G and R246I substitution in the NTD, also a L242H substitution or L242-244 del is present. The CTD contains a K417N, E484K and N501Y substitution[28,32,33]. Besides the N501Y mutation which is associated with enhanced transmission[30,34], the E484K mutation is the most concerning mutation for reduced neutralization by monoclonal antibodies and plasma from patients that were infected with SARS-CoV-2 before[35–37]. The mutant used in this report contains a D80A, D215G and a

L242H mutation in the NTD and a K417N, E484K and N501Y mutation in the CTD. Furthermore, a variant of B.1.351 with an additional R246I mutation in the NTD (B.1.351 R246I) is also investigated since this mutation is believed to play a key role in the escape from some neutralizing antibodies[38–41]. The P.1 variant (gamma) identified in Brazil in November 2020 has a L18F, T20N, P26S, D138Y and a R190S substitution in the NTD. Notably, the mutant used in this report contained no mutations in the NTD and therefore was identical to wt SARS-CoV-2. In the CTD, a K417T, E484K and N501Y mutation are detected[28,42]. These mutations were all present in the mutant used here. Some of these mutations overlap with the B.1.1.7 and B.1.351 variant, therefore the same effects on transmissibility and antibody and immune evasion as for the other two variants are plausible. Little additional information about the effects of the mutations in this variant is known. All three variants have also been associated with a more severe disease course[43–45]. The fourth VOC is the B.1.617.2 variant (delta), identified in India in October 2020[26]. This variant was not studied as it arose later during this internship.

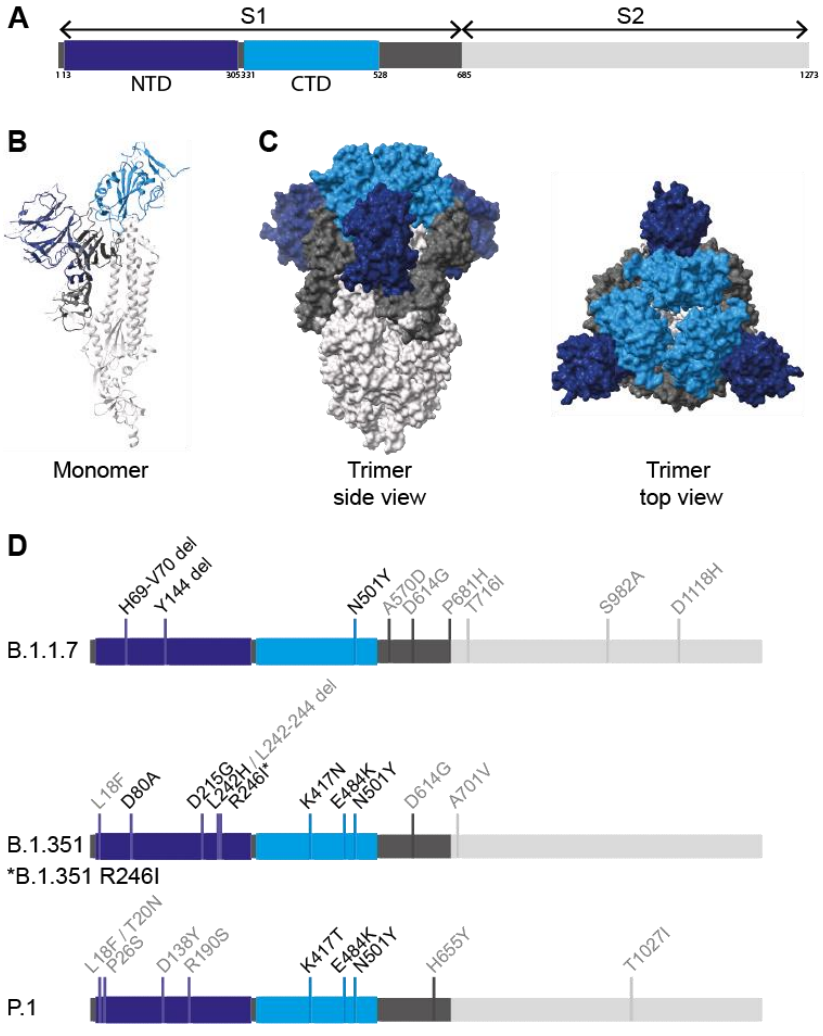

Figure 1: Overview of SARS-CoV-2 spike protein and VOC mutations. A Schematic overview of SARS-CoV-2 spike protein domains. The S1 (except NTD (dark blue) and CTD (light blue)) is displayed in dark grey and the S2 in light grey. **B** Side view of monomeric subunit of the spike protein shown in ribbons, the same color scheme as in A is used (PDB entry 6vxx, adapted with ChimeraX). **C** Side view and top view of the trimeric spike shown as a surface. The same color scheme as in A and B is used (PDB entry 6vxx, adapted with ChimeraX). **D** Schematic overview of the mutations in the SARS-CoV-2 spike proteins of the VOCs, black mutations are present in the mutants used in this report, grey mutations are also variant-defining, but not present in the mutants used in this report.

Host range of SARS-CoV-2

It is known that SARS-CoV-2 can infect several animal species like ferrets, minks, and Syrian hamsters[46]. Studies have shown that SARS-CoV-2-wt-CTD showed specific binding to the terminal bronchiolar structures and alveoli of ferret lung tissues[47] and that SARS-CoV-2 is transferrable between ferrets via contact and through the air[48,49]. Other animal models, such as guinea pigs have been proven to be susceptible for SARS-CoV-1[50,51], but whether SARS-CoV-2 can also infect guinea pigs, is not known yet. Protein models predict potential binding of SARS-CoV-2 to the guinea pig ACE2, nonetheless the binding mode seems to be substantially different from the binding of SARS-CoV-2 to human ACE2[52]. Until now, the most suitable animal model for SARS-CoV-2 infection studies is the Syrian hamster. Like ferret lung tissues, SARS-CoV-2-wt-CTD showed binding to terminal bronchiolar structures of Syrian hamster lung tissues with a significantly higher intensity than for SARS-COV-1-wt-CTD[47]. Besides, they can become infected in experimental settings and show symptoms such as respiratory distress[53]. Virus replication also seems to be high in those animals, especially in the lower respiratory tract[46,54]. Piglets are shown to be unsusceptible to the virus in nature[55,56], yet some research suggests that pigs are to a low level susceptible to SARS-CoV-2 upon experimental infection and that sometimes immune responses are observed[57,58]. Furthermore, SARS-associated viruses have been previously detected in pigs[59,60], making it an interesting animal to consider for host range extension by SARS-CoV-2 variants, as this can occur upon changes in the receptor binding site or be a consequence of newly introduced binding sites[61–67]. Mice seem to be unsusceptible to infection because of the disability of the SARS-CoV-2 spike protein to efficiently bind to the mouse orthologue of ACE2[13,68]. However, a host range extension to mice is already suggested for VOC B.1.351 and P.1[69], therefore mice are interesting to further investigate the different VOCs.

In this report, monomeric and trimeric NTDs and CTDs of HCoVs and VOCs were cloned and expressed to be of use in a range of biological assays (cell staining, tissue staining, glycan and heparan sulphate arrays and formation of virus-like particles). Binding properties of the NTD and CTD of VOC P.1, B.1.1.7, B.1.351 and B.1.351 R246I to cultured VERO-E6 cells and paraffin embedded lung tissues of several animal models were investigated and compared to wt SARS-CoV-2. The results demonstrate that P.1-CTD and B.1.1.7-CTD are suggested to be superior in tissue binding compared to wt SARS-CoV-2. Furthermore, binding studies of B.1.351-NTD and B.1.351 R246I-NTD suggested a possible binding site in these protein domains. Finally, all VOCs indicated a host range extension to mice, where P.1-CTD, B.1.1.7-CTD, B.1.351-NTD an B.1.351 R246I-NTD showed binding to mouse lung tissue slides.

RESULTS

Monomers and trimers of HCoVs and VOCs were made to use in several biological assays. Monomeric proteins without Spytag were expressed to use later in glycan and heparan sulphate array analysis and monomeric proteins with a Spytag were cloned for another project, so that a virus-like particle could be made. For cell and tissue staining, trimeric proteins were favourable over monomeric proteins, as the native coronavirus spike is a trimer.

A range of monomeric VOCs and HCoVs are efficiently expressed

To express recombinant monomeric protein domains with and without Spytag and fluorescent properties, plasmids containing an mOrange, an optional Spytag and a Strep-tag sequence were designed (figure 2A). All monomeric VOCs were efficiently expressed in HEK293T cells and could be detected in the cell culture supernatant (figure 2B). Expression of B.1.1.7-NTD and P.1-NTD with and without Spytag was comparable to wt-SARS-CoV-2. B.1.351-NTD with the Spytag domain showed a lower expression rate than B.1.351-NTD without Spytag domain. In contrast, the Spytag domain increased the expression yields for B.1.351 R246I-NTD. Overall, the NTDs did express much better than the CTDs, displaying thicker protein bands. Especially B.1.1.7-CTD and P.1-CTD showed a low expression yield. B.1.351-CTD (and the

identical B.1.351 R246I-CTD) with and without Spytag showed a similar expression as wt SARS-CoV-2-CTD. The fluorescence in the cell culture supernatant was also measured (figure 2C), confirming the expression yields detected on western blot. The fluorescence showed that for most proteins the Spytag domain causes a slight decrease in expression yield, whereby B.1.351 R246I-NTD is an exception. Here, the expression yields showed a significant increase in the presence of the Spytag domain.

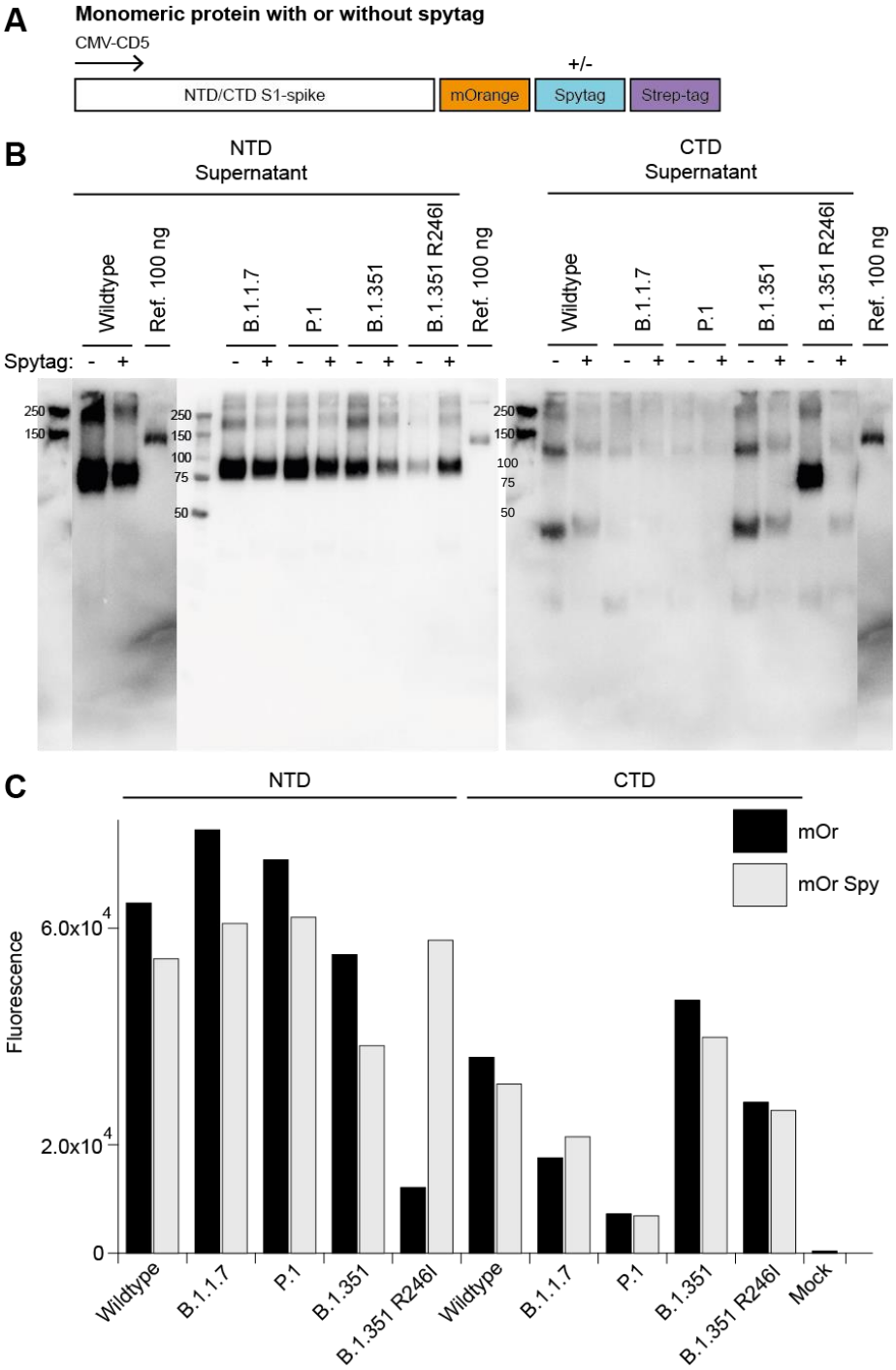

Figure 2: Western blot and fluorescence of monomeric VOC-NTDs and CTDs supernatant. A Schematic overview of used expression vector. **B** Western blot of monomeric NTDs and CTDs of the VOCs expressed in HEK 293T cells with and without a Spytag sequence. For each protein, an equal volume of supernatant was loaded onto the gel. **C** Bar plot of the mOrange emission measured in the supernatant of the proteins.

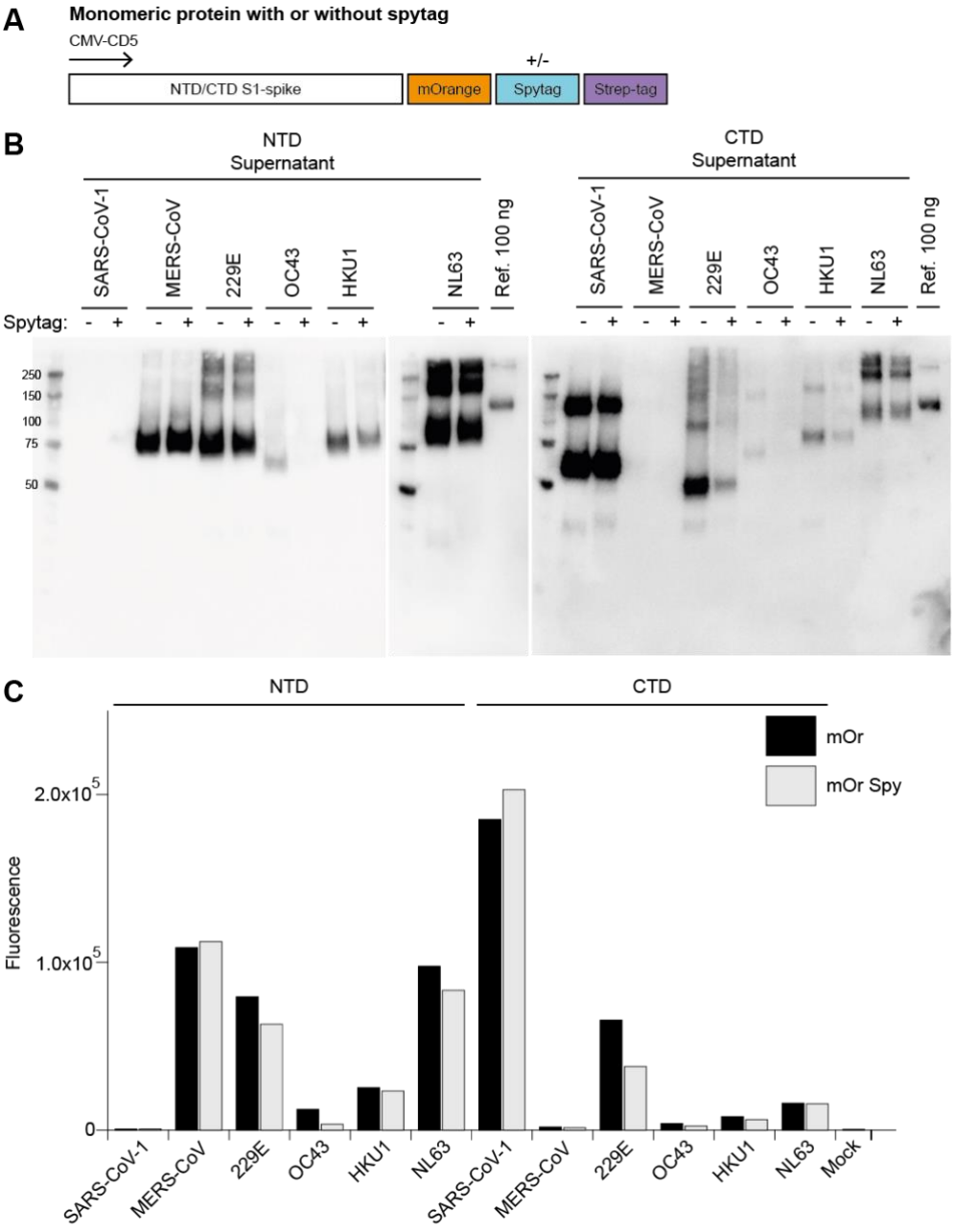

Figure 3: Western blot and fluorescence of monomeric HCoV-NTDs and CTDs supernatant. A Schematic overview of used expression vector. **B** Western blot of monomeric NTDs and CTDs of the HCoVs expressed in HEK 293T cells with and without a spytag sequence. For each protein, an equal volume of supernatant was loaded onto the gel. **C** Bar plot of the mOrange emission measured in the supernatant of the proteins.

For the other monomeric HCoV proteins, the same plasmids were used as for the monomeric VOCs (figure 3A). The cell culture supernatant was checked for expression on western blot (figure 3B). SARS-CoV-1-NTD with and without Spytag, MERS-CoV-CTD with and without Spytag and OC43-NTD and CTD with Spytag were not visible on western blot. The other proteins could be detected in the supernatant, whereby MERS-CoV-NTD, 229E-NTD, NL63-NTD, SARS-CoV-1-CTD with and without Spytag, showed very high expression yields. For, 229E-CTD, the protein without a Spytag domain showed a significantly higher expression compared to the protein with Spytag domain. Fluorescence measurements of the cell culture supernatant (figure 3C) confirmed the expression yields detected on western blot, only the difference for 229E-CTD with and without Spytag domain, was less significant than on western blot.

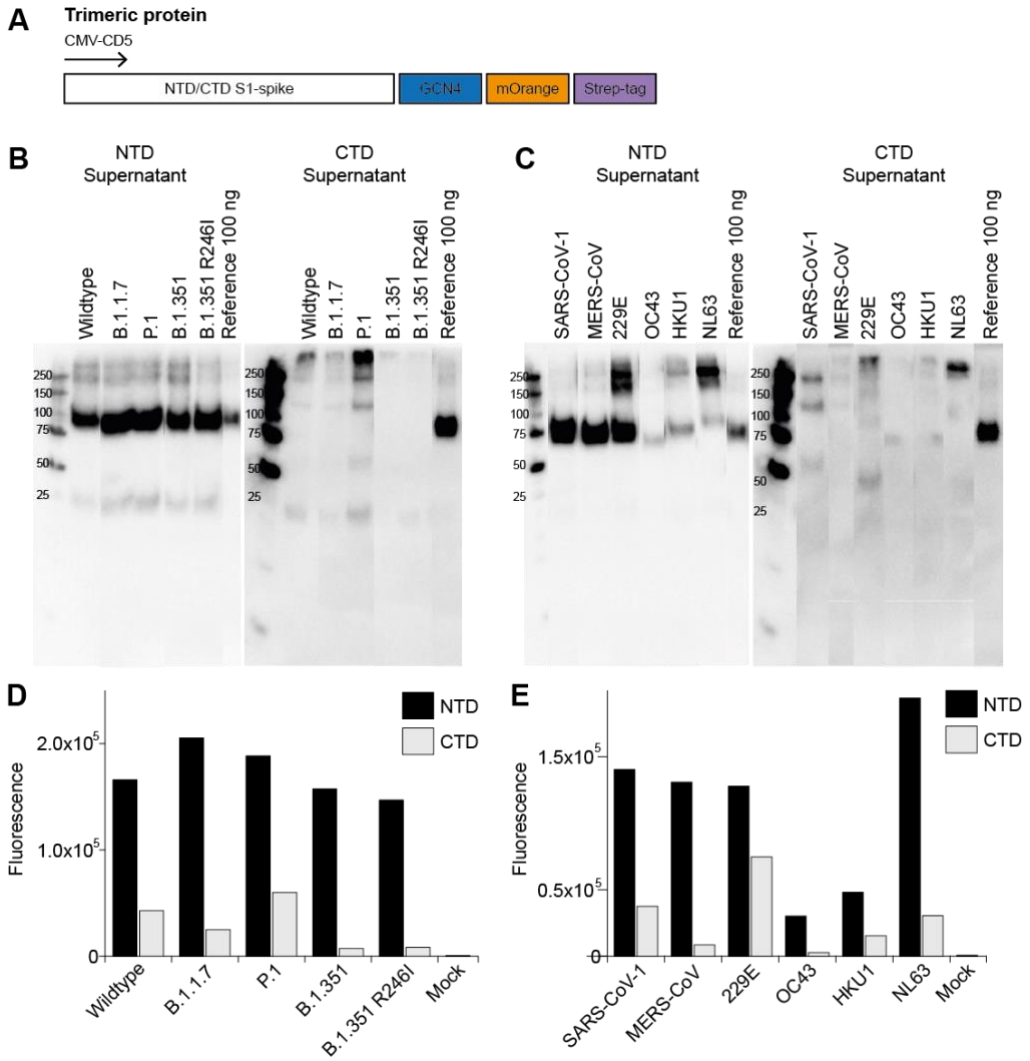

Figure 4: Western blot and fluorescence of trimeric HCoV and VOC-NTDs and CTDs supernatant. A Schematic overview of used expression vector. **B** Western blot of trimeric NTDs and CTDs of the VOCs expressed in in HEK 293T cells. For each protein, an equal volume of supernatant was loaded onto the gel. **C** Western blot of trimeric NTDs and CTDs of the HCoVs expressed in HEK 293T cells. For each protein, an equal volume of supernatant was loaded onto the gel. **D** Bar plot of the mOrange emission measured in the supernatant of the VOC proteins. **E** Bar plot of the mOrange emission measured in the supernatant of the hCoV proteins.

A range of trimeric VOCs and HCoVs are efficiently expressed

To express recombinant trimeric protein domains with fluorescent properties, a plasmid containing an GCN4 trimerization domain, an mOrange and a Strep-tag sequence was designed (figure 4A). All proteins, except for OC43-CTD were visible on western blot. The NTD-VOCs all showed a high expression yield similar to wt SARS-CoV-2. Like the monomeric expression, the trimeric NTDs expressed much better compared to the CTDs. B.1.351-CTD (and the identical B.1.351 R246I-CTD) displayed a very low expression yield, however, for the biological assays enough protein was obtained. P.1-CTD showed a significant higher expression yield compared to the wt. These observations were confirmed by the fluorescence measurements of the cell culture supernatant (figure 4D). For the trimeric HCoVs (expressed using the same plasmid as for the trimeric VOCs) similar expression yields as for the monomeric proteins were observed (figure 4B). Notably, trimeric SARS-CoV-1-NTD did show significant expression and SARS-CoV-1-CTD did only show very weak expression, in contrast with the expression yields seen for monomeric SARS-CoV-1. Fluorescence measurements of the cell culture supernatant were in agreement with the expression yields detected on western blot (figure 4E).

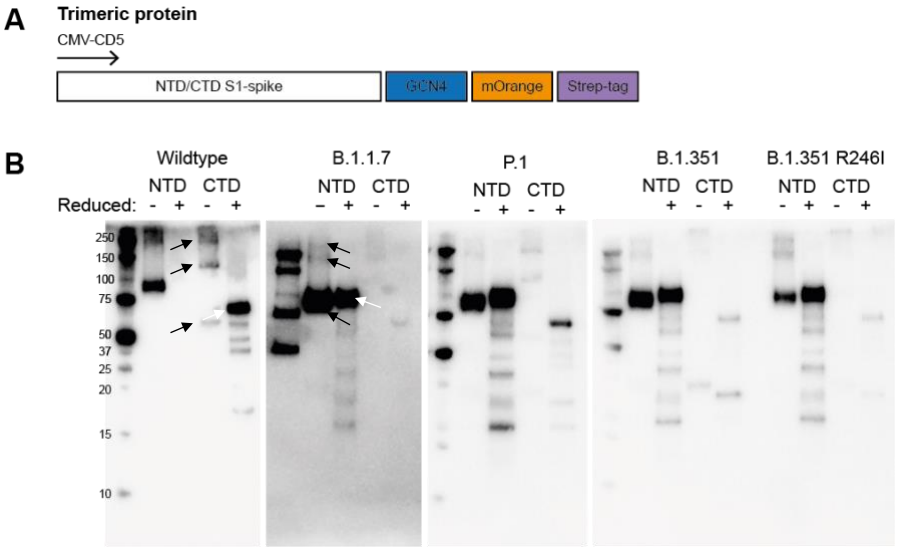

Figure 5: Western blot of purified VOC-NTDs and CTDs. A Schematic overview of used expression vector. **B** Western blot of purified trimeric NTDs and CTDs of the VOCs. Black arrowheads display monomeric, dimeric and trimeric fractions of non-reduced samples. White arrowheads display monomeric fractions of reduced samples. For each protein, an equal concentration of protein was loaded onto the gel.

The trimeric proteins were purified and further analysed on western blot (figure 5 and supplementary figure 1). Non-reduced protein samples showed monomeric, dimeric, and trimeric fractions (see black arrowheads in figure 5). After reduction, those fractions were all reduced to monomeric fractions (see white arrowheads in figure 5). All VOCs displayed the same electrophoretic mobility compared to the SARS-CoV-2-wt, indicating that the proteins were expressed similar to the wt. NTDs showed a higher concentration on the western blot than the CTDs, even though an equal concentration of each protein was loaded onto the gel. Furthermore, the reduced sample of SARS-CoV-2-wt-NTD was not visible on the western blot. However, previous research already showed reduction of dimeric and trimeric fractions to monomeric fractions[47].

Immunofluorescent cell staining shows binding of several domains to VERO-E6 cells

To get a first indication of the binding properties of the proteins of interest, VERO-E6 cells were stained with the VOC-NTD and VOC-CTD proteins (figure 6), as VERO-E6 cells are known to support SARS-CoV-2[70]. Binding to VERO-E6 cells was observed using SARS-CoV-2-wt-CTD, which is known to contain a receptor binding domain in its CTD[19]. B.1.1.7-CTD and P.1-CTD also showed binding, where P.1-CTD showed an increased intensity and B.1.1.7-CTD showed a decreased intensity compared to wt-CTD. No binding was observed for B.1.351-CTD (and

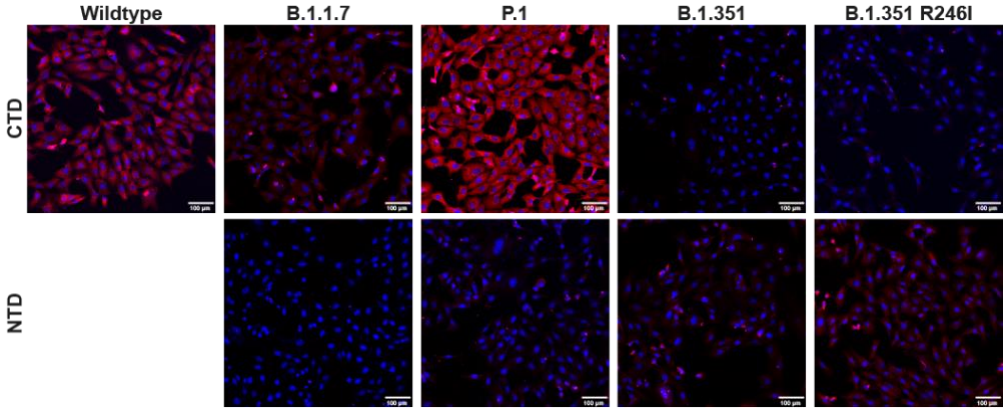

Figure 6: Staining VERO E6 cells with variants of concern. VERO E6 cells were stained using CTD and NTD S1-spike proteins of the VOCs. Proteins were applied at 50 µg/ml.

the identical B.1.351 R246I-CTD). In addition, the NTDs of the current VOCs were applied to investigate their binding properties. No binding was observed for B.1.1.7-NTD and P.1-NTD, showed very weak binding. B.1.351-NTD and B.1.351 R246I-NTD displayed binding to VERO-E6 cells with a slightly higher intensity.

P.1-CTD and B.1.1.7-CTD show superior binding properties

To further determine whether the CTDs of the current VOCs are responsible for attachment prior to infection like wt SARS-CoV-2, ferret, piglet, mouse, Syrian hamster, and guinea pig lung tissue slides were stained with the protein domains (figure 7). Before staining, all but guinea pig tissues were validated, whereby biological properties were confirmed (supplementary figure 2). Specific binding of the SARS-CoV-2 wt-CTD to bronchiolar structures of the ferret, piglet, guinea pig and Syrian hamster lungs was observed. Particularly, in the ferret lungs only the tertiary bronchiolar structures were bound by the wt-CTD, whereas to the primary and secondary bronchiolar structures no binding was observed (supplementary figure 3). In addition, binding towards alveolar cells of the piglet, Syrian hamster and guinea pig lungs was observed using wt-CTD. Furthermore, wt-CTD showed weak binding properties towards the arterial pulmonary vessels of the guinea pig lungs. As a negative control, mouse lungs were included as no infection of wt SARS-CoV-2 has been reported yet. As expected, wt-CTD did not show any binding to these lungs. By applying the VOC-CTDs, an increased intensity of P.1-CTD and B.1.1.7-CTD to ferret, piglet and guinea pig lung tissues was observed, compared to wt-CTD. For the ferret lung tissues, binding of P.1-CTD to primary and secondary bronchiolar structures was detected, in contrast to wt-CTD (supplementary figure 3). P.1-CTD also showed an increased signal upon binding to the hamster lungs and B.1.1.7-CTD (n=1) showed similar binding as for the wt-CTD. Furthermore, specific binding to the mouse lung was detected in the tertiary bronchioles and alveoli when stained with P.1-CTD and B.1.1.7-CTD. In contrast, B.1.351-CTD (and the identical B.1.351 R246I-CTD) showed a decreased binding to ferret, piglet, and guinea pig lung tissue slides. These variants did show some specific binding to the alveoli of the mouse lungs.

B.1.351-NTD and B.1.351 R246I-NTD have binding properties

To further investigate the binding properties of the NTD-VOCs, all previously described lung tissues were stained with the NTDs (figure 8). No binding was observed using the wt-NTD, except for the guinea pig lung, where minimal binding to the bronchiolar structures was detected. Minor staining was detected using B.1.1.7-NTD and P.1-NTD to the alveolar cells of the mouse lung. No binding was observed for wt-NTD, B.1.1.7-NTD and P.1-NTD. In contrast, intense and specific binding to the bronchiolar structures of all animal tissues was observed using B.1.351-NTD and B.1.351 R246I-NTD where binding to the smaller bronchiolar structures of ferret lungs was detected. In addition, binding to the alveolar cells of mouse and Syrian hamster lungs and binding to the lung vessels and alveolar cells of guinea pig tissue was observed.

DISCUSSION

In this report, differences in binding properties of several NTDs and CTDs of the S1-spike protein of SARS-CoV-2 VOCs to VERO-E6 cells and to lung tissues of model animal species was demonstrated. The P.1-CTD and B.1.1.7-CTD bound with a higher intensity to VERO-E6 cells, ferret, piglet, Syrian hamster, and guinea pig lung tissues compared to wt SARS-CoV-2. Furthermore, an indication for a binding site in the B.1.351-NTD and B.1.351 R246I-NTD was observed. Lastly, all variants showed binding of one of the domains to mice lung tissues, suggesting a host range extension.

Binding assays of VOC P.1-CTD and B.1.1.7-CTD indicated a superior binding of these variants over SARS-CoV-2-wt-CTD (figure 6 and 7). Supportive to the observations, the N501Y mutation seen in both variants is associated with enhanced binding abilities to ACE2[30,31,63]. The E484K mutation which is only present in P.1, is responsible for reduced antibody

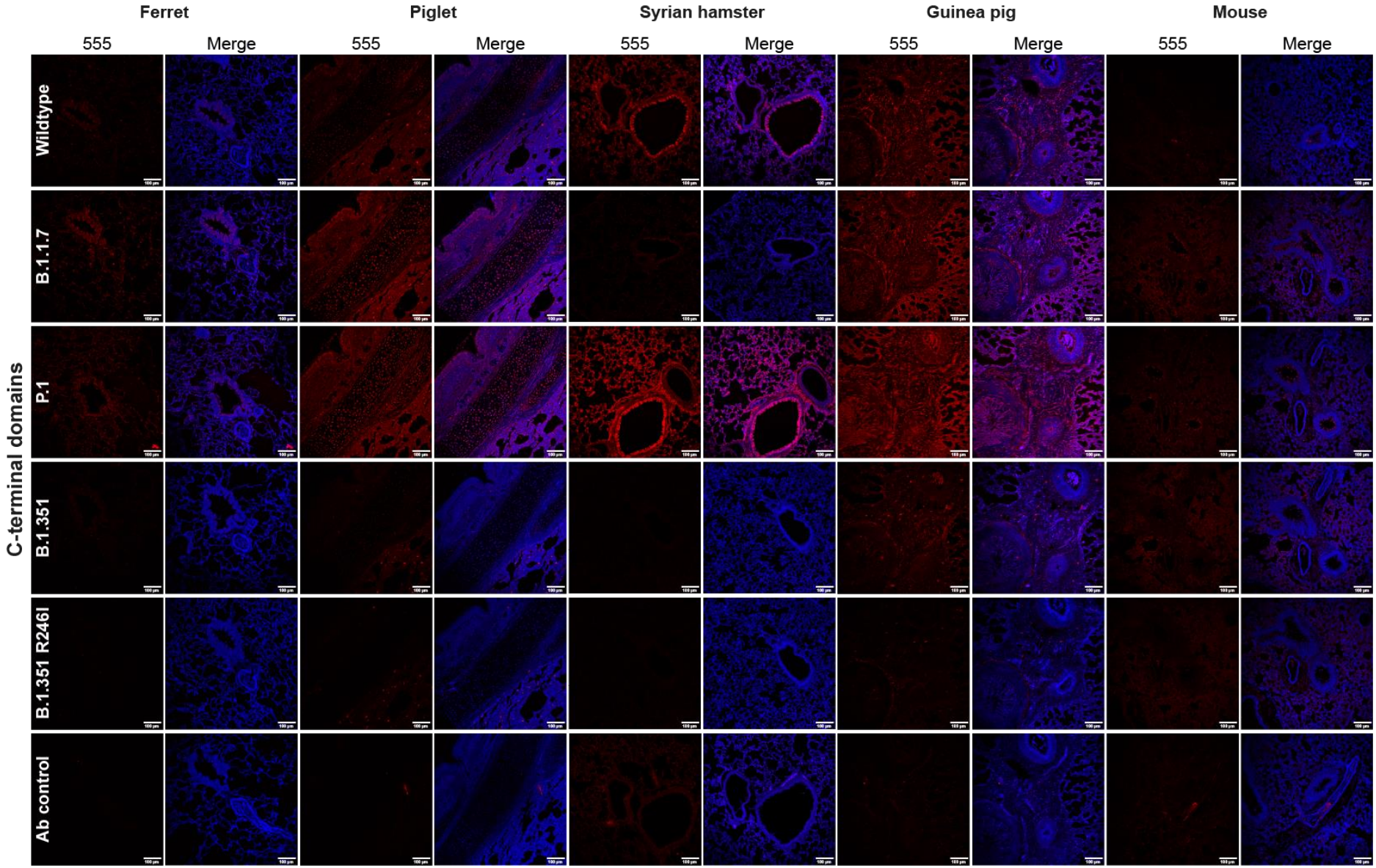

Figure 7: Staining of lung tissues with CTDs of variants of concern Ferret, piglet, Syrian hamster, guinea pig and mouse formalin fixed paraffin embedded lung tissue slides were stained using the CTD of the VOCs. Proteins were applied at 50 µg/ml.

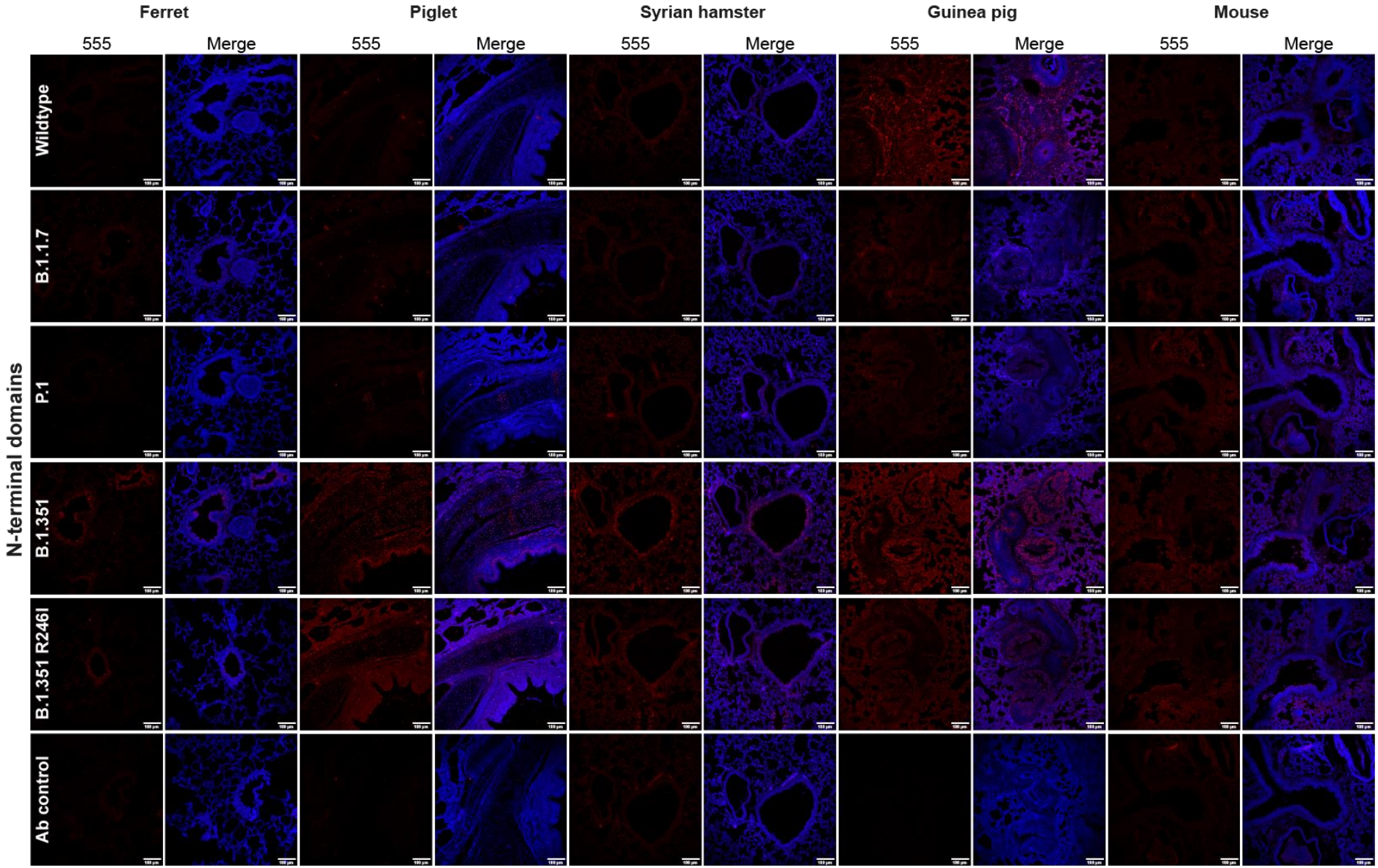

Figure 8: Staining of lung tissues with NTDs of variants of concern Ferret, piglet, Syrian hamster, guinea pig and mouse formalin fixed paraffin embedded lung tissue slides were stained using the NTD of the VOCs. Proteins were applied at 50 µg/ml.

binding[35–37], but has also been demonstrated to enhance ACE2 binding to a lesser extend[63,71]. Interestingly, the K417T mutation, present in P.1-CTD, is considered to reduce binding to ACE2[61,71,72], suggesting a stronger binding affinity for B.1.1.7-CTD compared to P.1-CTD. This is contradictory to the observed staining intensity of the VERO-E6 staining experiments. For the tissue staining experiments no major differences were observed, except for the hamster lung tissues. However, since the images used for this model animal were not from the same experiment, intensities of the staining can differ, and no comparison can be made. Most literature suggests that B.1.1.7 binds slightly stronger to ACE2 compared to P.1. Nonetheless, no binding studies to cells or tissues were performed in these studies, only 1:1 binding assays for ACE2 and SARS-CoV-2 binding sites were done with monomeric proteins [63,71,73,74], whereas trimeric proteins were used in this study. To better investigate the specific role of each mutation in cell and tissue binding properties, single mutations should be introduced and tested.

B.1.351-CTD (and the identical B.1.351 R246I-CTD) showed weak binding intensity to VERO-E6 cells compared to wt-CTD (figure 6). Similar results were obtained for the tissue staining experiments of ferret, piglet, guinea pig, and mouse lung tissues (figure 7). Considering the mutations present in B.1.351-CTD (N501Y, E484K and K417N), a similar binding intensity as for P.1-CTD (N501Y, E484K and K417T) was expected, since K417N and K417T share the same properties. Yet, this was not observed in this study. Several computational and experimental studies report similar affinity scores for the binding of both variants to ACE2[75,76]. However, other studies report a slightly higher binding affinity for P.1. For instance, Barton M. I. *et al.* reported a 3.7-fold increased affinity for B.1.351 and a 5.3-fold increase for P.1, compared to the wt-spike protein, whereby the study was conducted with monomeric forms of the CTD and ACE2[72]. This might partly explain the observed differences in fluorescent intensity of P.1-CTD and B.1.351-CTD. Furthermore, it was noticed that B.1.351-CTD degrades over time, and staining experiments done with older proteins showed a lower intensity than in experiments using a newly expressed protein batch. Degradation was confirmed by SDS-page analyses. This is coherent with the low expression rates of B.1.351-CTD (figure 4 and 5) since lower concentrations of protein can result in a faster degradation. Therefore, the staining results of B.1.351-CTD must be interpreted with caution.

Another observation made, was the binding intensity of B1.351-NTD and B.1.351 R246I-NTD for VERO-E6 cells (figure 6) and all model animal lung tissues (figure 8). The wt-NTD also showed minor binding for guinea pig lung tissues (n=2). The observed binding intensities suggest a possible binding site in the NTD of these variants. N-terminal binding sites are seen before in other human coronaviruses, such as in OC43, HKU1 and MERS-CoV[20–23]. These binding domains are sialic acid binding domains and are crucial in infection. Possibly, a same type of binding site is present in the B.1.351-NTD and B.1.351 R246I-NTD. In addition to this data, sialic acid recognition of the SARS-CoV-2 spike, is proposed before with the help of a glyconanoparticle platform[77] and molecular dynamics simulation of the NTD of wt SARS-CoV-2 together with a sialic acid molecule, showed short-lived binding events[78]. Considering that other viruses, such as influenza viruses, have shown switching of sialic acid binding properties before[79,80], underlining the importance of sialic acid binding in infection, it is plausible that variants of the SARS-CoV-2 spike develop stronger sialic acid binding properties over time. Recent research also showed that NTD insertions seen in several VOCs are close to the loop regions that are likely to be involved in sialic acid binding and increases in predicted sialic acid binding energies were proposed for some VOCs[81]. The R246I mutation did not cause a big difference upon binding. In VERO-E6 cells, binding was comparable, for tissues the B.1.351 variant without the R246I mutation seemed to bind stronger, however this increased intensity was minimal for piglet and mouse lungs.

Besides an increased binding affinity or a newly introduced binding site, a virus can extend its host range upon changes in its binding domain[62,64–67]. Until now, no infection of wt SARS-

CoV-2 in mice has been reported yet. This was in agreement with the obtained data in this report (figure 7 and 8). In contrast, P.1-CTD, B.1.1.7-CTD, B.1.351-NTD and B.1.351 R246I-NTD showed binding to mice lung tissues (figure 7 and 8). Supporting an expansion of the host range to mice. In addition to our data, Yao W. *et al.* showed the ability of P.1, B.1.1.7 and B.1.351 to enter cells by the rat and mouse orthologue of ACE2[82] and Montagutelli X. *et al.* suggested infection of laboratory mice with the P.1 and B.1.351 lineages, yet infection with the B.1.1.7 lineage was not reported[69]. Even though, there is no guarantee that observed binding intensities are in agreement with the ability of a virus to infect an animal in nature, tissue staining experiments can be a supportive tool to predict host ranges.

The new insights into the binding abilities of several S1-spike domains of the SARS-CoV-2 VOCs to various animal model tissues provided in this research, can be of help by development of vaccines, and inhibitory antibodies, as it gives a better understanding of the binding abilities. Besides this, it provides grounds to use mice as an animal model for research to several VOCs. In addition, further research to the B.1.351 lineage, that seems to have gained a binding site in the NTD of the S1-spike protein, can provide a better understanding of the binding mode of the investigated VOCs.

MATERIALS AND METHODS

Cloning of expression vectors

Plasmids containing the open reading frame of four different SARS-CoV-2 VOC spike proteins, P.1, B.1.1.7, B.1.351 and B.1.351 R246I were kindly provided by Tom Caniels, Marit van Gils and Rogier Sanders of the Amsterdam Medical Centre. The NTDs (AA position 26 to 318, UniProtKB – P0DTC2) and CTDs (AA position 319 to 541, UniProtKB – P0DTC2) were amplified using PCR (Q5 Site-Directed Mutagenesis Kit, New England Biolabs, E0554) with an annealing temperature of 60 °C for B.1.351, B.1.351 R246I and B.1.1.7 and 63.9 °C for P.1. Afterwards, the PCR products were cloned into a pCD5 expression vector using the Gibson Assembly Cloning Kit (New England Biolabs, E5510S). The pCD5 vector used for expression of monomeric protein domains with and without Spytag also contained sequences coding for a secretion signal, a Tobacco Etch Virus (TEV) cleavage site, an mOrange2 fluorescent protein, a Spytag (optional) and a Twin-Strep. The pCD5 vector used for expression of trimeric protein domains also contained sequences coding for a GCN4 trimerization domain, a secretion signal, a Tobacco Etch Virus (TEV) cleavage site, a mOrange2 fluorescent protein and a Twin-Strep. The obtained Gibson products were transformed into MC1061 competent *E. coli* cells and grown overnight on LB agar plates (2x YT, 46 g/L) containing ampicillin (50 µg/ml) and tetracycline (10 µg/ml). Several colonies were picked and grown in new medium (LB-medium, 31 g/L) also containing ampicillin (50 µg/ml) and tetracycline (10 µg/ml). To determine if the clones contained the correct insert, plasmids were purified using a QIAprep Spin Miniprep Kit (QIAGEN, 27104) and afterwards digested using restriction enzymes NheI (New England Biolabs, R0131) and PacI (New England Biolabs, R0547S). Plasmids containing an insert of the right size were also sanger-sequenced for verification.

Protein expression and purification

After the DNA was verified, the different HCoV and VOC-containing plasmids were transfected into 50-60% confluent HEK293T cells. DNA was incubated for 20 minutes with polyethyleneimine I (PEI, linear 25 kDa, Polysciences, 02371) with a ratio of 1:23.7 g/g and Dulbeccos Modified Eagles Medium (DMEM, Gibco, 11965084). After 6 hr incubation, the transfection mix was replaced with 293 SFM II expression medium (Gibco, 11686029), supplemented with sodium bicarbonate (3.7 g/L), glucose (2.0 g/L), Primatone RL-UF (3.0 g/L), glutaMAX (Gibco, 35050061), valproic acid (2 mM), and DMSO (1,5%).

Four days after transfection, the supernatant of the cells was harvested. The fluorescence was measured with a POLARstar fluorescent reader (555 nm and 590 nm). Supernatant with a fluorescent signal lower than 40.000 RFU was concentrated. In addition, expression was

confirmed by western blot using a StrepMAB classic-HRP antibody (Iba, 2-1509-001). Proteins were purified using StrepTactin Sepharose beads in PBS (Iba, 2-1201-002). Purified trimeric proteins were further analysed on western blot using a reduced sample and a non-reduced sample, all containing 100 ng protein. Reduction was done by adding 4 µL DTT to the protein and incubated for one hour at 100 °C prior to SDS-page.

Cell and tissue preparation

VERO-E6 cells were grown on coverslips to 70-80% confluency. Then cells were washed using PDB and fixed using 4% paraformaldehyde (Thermo Fisher Scientific, J61899) in PBS for 20 min at RT. After fixation, the coverslips with cells were stored in PBS at 4°C or directly used for fluorescent staining.

Formalin fixed lung tissues from different model animals were obtained from the department of Veterinary Pathobiology, Faculty of Veterinary Medicine, Utrecht University, and the department of Viroscience, Erasmus University, The Netherlands. Tissues were embedded in paraffin blocks and sectioned at 0.4 µm using a microtome and dried on glass slides overnight at 37 °C. Afterwards, they were stored at 4 °C.

Immunofluorescent cell and tissue staining

The fixed cells on coverslips were first permeabilized with 0,1% Triton-X100 (Sigma-Aldrich, 10789704001) diluted in PBS. Cells were incubated with 3% BSA in PBS for 30 min at RT. The proteins (50 µg/ml) were added to the cells for 1 hr at RT. Primary antibody used was Strep-Mab classic chromeo-564, 2 µg/ml (Iba, 2-1550-050) and secondary antibody used was Goat anti-mouse Alexa-fluor 555, 4 µg/ml (Invitrogen, A21422), cells were incubated with the antibodies for 1 hr and 45 min respectively. DAPI (Invitrogen, 10236276001) was used as nuclear staining. In between the antibody staining steps, cells were washed twice with 0.05% PBS-Tween. Before adding the DAPI, cells were washed twice with 0.05% PBS-Tween and once with PBS, and afterwards cells were washed twice with milliQ water. Coverslips were mounted using FluorSave reagent (Merck Millipore, 345789) and dried overnight in the dark at RT before imaging.

Tissue slides were deparaffinized in xylene. Rehydration was established using 100%, 96% and 70% alcohol and demi water respectively. Afterwards the tissues were boiled in a pre-warmed citrate buffer of pH 6.0 for 10 min at 900 kW in the microwave for antigen retrieval and washed three times in PBS-Tween. Endogenous peroxidase activity was blocked using 1% hydrogen peroxide in methanol for 30 min. Tissues were incubated overnight with 3% BSA in PBS at 4 °C. Protein binding and antibody, nuclear staining and coverslip attachment steps were the same as for the cell staining, washes in between the steps were performed with PBS.

Sample imaging

Samples were imaged on a Leica SPE-II – DMI4000 confocal microscope at the Centre for Cell Imaging, Utrecht University. The objective used was a 10x ACS Apo (N.A. 0.30). Excitation wavelength for DAPI was 405 nm and to visualize protein binding excitation wavelength was 561 nm. Emission was obtained in the range of 566-620 nm. Laser power used for DAPI imaging was 20% and for primary and secondary antibodies 37%, with a gain of 1110.0. Merging of different imaged channels, addition of scale bars and brightness adjustment of the DAPI channel were done with ImageJ version 1.53c.

REFERENCES

1. Weiss, S. R. & Leibowitz, J. L. Coronavirus Pathogenesis. *Advances in Virus Research* **81**, 85–164 (2011).
2. Payne, S. Family Coronaviridae. *Viruses* 149 (2017) doi:10.1016/B978-0-12-803109-4.00017-9.
3. Pillaiyar, T. *et al*. Recent discovery and development of inhibitors targeting coronaviruses. *Drug Discovery Today* **25**, 668–688 (2020).
4. Chen, B. *et al.* Overview of lethal human coronaviruses. *Signal Transduction and Targeted Therapy 2020 5:1* **5**, 1–16 (2020).
5. Hoek, L. van der *et al.* Identification of a new human coronavirus. *Nature Medicine* **10**, 368 (2004).

6. Hamre, D. & Procknow, J. J. A New Virus Isolated from the Human Respiratory Tract. *Proceedings of the Society for Experimental Biology and Medicine* **121**, 190–193 (2016).
7. Woo, P. C. Y. *et al.* Characterization and Complete Genome Sequence of a Novel Coronavirus, Coronavirus HKU1, from Patients with Pneumonia. *Journal of Virology* **79**, 884 (2005).
8. Zhong, N. *et al.* Epidemiology and cause of severe acute respiratory syndrome (SARS) in Guangdong, People's Republic of China, in February, 2003. *Lancet (London, England)* **362**, 1353 (2003).
9. Zhou, P. *et al.* A pneumonia outbreak associated with a new coronavirus of probable bat origin. *Nature 2020 579:7798* **579**, 270–273 (2020).
10. Zaki, A. M. *et al*. Isolation of a Novel Coronavirus from a Man with Pneumonia in Saudi Arabia. *The New England Journal of Medicine* **367**, 1814–1820 (2012).
11. McIntosh, K. *et al.* Recovery in tracheal organ cultures of novel viruses from patients with respiratory disease. *Proceedings of the National Academy of Sciences of the United States of America* **57**, 933 (1967).
12. Zhu, N. *et al.* Brief Report: A Novel Coronavirus from Patients with Pneumonia in China, 2019. *The New England Journal of Medicine* **382**, 727 (2020).
13. Zhou, P. *et al.* A pneumonia outbreak associated with a new coronavirus of probable bat origin. *Nature* **579**, 270–273 (2020).
14. WHO Coronavirus (COVID-19) Dashboard | WHO Coronavirus (COVID-19) Dashboard With Vaccination Data. https://covid19.who.int/. *last visited 08-07-2021.*
15. Bernal, J. L. *et al.* Effectiveness of Covid-19 Vaccines against the B.1.617.2 (Delta) Variant. *The New England Journal of Medicine* (2021) doi:10.1056/NEJMOA2108891.
16. Forni, G. & Mantovani, A. COVID-19 vaccines: where we stand and challenges ahead. *Cell Death & Differentiation 2021 28:2* **28**, 626–639 (2021).
17. Hoffmann, M. *et al.* SARS-CoV-2 Cell Entry Depends on ACE2 and TMPRSS2 and Is Blocked by a Clinically Proven Protease Inhibitor. *Cell* **181**, 271 (2020).
18. Huang, Y. *et al.* Structural and functional properties of SARS-CoV-2 spike protein: potential antivirus drug development for COVID-19. *Acta Pharmacologica Sinica 2020 41:9* **41**, 1141–1149 (2020).
19. Wang, Q. *et al.* Structural and Functional Basis of SARS-CoV-2 Entry by Using Human ACE2. *Cell* **181**, 894-904.e9 (2020).
20. Huang, X. *et al.* Human Coronavirus HKU1 Spike Protein Uses O -Acetylated Sialic Acid as an Attachment Receptor Determinant and Employs Hemagglutinin-Esterase Protein as a Receptor-Destroying Enzyme . *Journal of Virology* **89**, 7202–7213 (2015).
21. Vlasak, R. *et al.* Human and bovine coronaviruses recognize sialic acid-containing receptors similar to those of influenza C viruses. *Proceedings of the National Academy of Sciences of the United States of America* **85**, 4526–4529 (1988).
22. Hulswit, R. J. G. *et al.* Human coronaviruses OC43 and HKU1 bind to 9-O-acetylated sialic acids via a conserved receptor-binding site in spike protein domain A. *Proceedings of the National Academy of Sciences* **116**, 2681–2690 (2019).
23. Li, W. *et al.* Identification of sialic acid-binding function for the Middle East respiratory syndrome coronavirus spike glycoprotein. *Proceedings of the National Academy of Sciences of the United States of America* **114**, E8508 (2017).
24. Cov-Lineages. https://cov-lineages.org/. *last visited 13-11-2021.*
25. Nextstrain / ncov / gisaid / global. https://nextstrain.org/ncov/gisaid/global.
26. Tracking SARS-CoV-2 variants. https://www.who.int/en/activities/tracking-SARS-CoV-2-variants/. *last visited 13-11-2021.*
27. SARS-CoV-2 variants of concern as of 14 October 2021. https://www.ecdc.europa.eu/en/covid-19/variants-concern. *last visited 13-11-2021.*
28. Caro, A. *et al.* Severe acute respiratory syndrome coronavirus 2 escape mutants and protective immunity from natural infections or immunizations. *Clinical Microbiology and Infection* **27**, 823 (2021).
29. Cov-Lineages. https://cov-lineages.org/global_report_B.1.1.7.html. *last visited 13-11-2021.*
30. Yang, T.-J. *et al.* Effect of SARS-CoV-2 B.1.1.7 mutations on spike protein structure and function. *Nature Structural & Molecular Biology 2021 28:9* **28**, 731–739 (2021).
31. Starr, T. N. *et al.* Deep Mutational Scanning of SARS-CoV-2 Receptor Binding Domain Reveals Constraints on Folding and ACE2 Binding. *Cell* **182**, 1295 (2020).
32. Cov-Lineages. https://cov-lineages.org/global_report_B.1.351.html. *last visited 13-11-2021.*
33. Tegally, H. *et al.* Emergence and rapid spread of a new severe acute respiratory syndrome-related coronavirus 2 (SARS-CoV-2) lineage with multiple spike mutations in South Africa. *medRxiv* **10**, 2020.12.21.20248640 (2020).
34. Starr, T. N. *et al.* Deep Mutational Scanning of SARS-CoV-2 Receptor Binding Domain Reveals Constraints on Folding and ACE2 Binding. *Cell* **182**, 1295-1310.e20 (2020).
35. Wang, P. *et al.* Antibody resistance of SARS-CoV-2 variants B.1.351 and B.1.1.7. *Nature 2021 593:7857* **593**, 130–135 (2021).
36. Greaney, A. J. *et al.* Comprehensive mapping of mutations in the SARS-CoV-2 receptor-binding domain that affect recognition by polyclonal human plasma antibodies. *Cell Host & Microbe* **29**, 463-476.e6 (2021).
37. Greaney, A. J. *et al.* Complete Mapping of Mutations to the SARS-CoV-2 Spike Receptor-Binding Domain that Escape Antibody Recognition. *Cell Host & Microbe* **29**, 44-57.e9 (2021).
38. Wang, P. *et al.* Increased Resistance of SARS-CoV-2 Variants B.1.351 and B.1.1.7 to Antibody Neutralization. *bioRxiv* (2021) doi:10.1101/2021.01.25.428137.

39. Mccallum, M. *et al.* N-terminal domain antigenic mapping reveals a site of vulnerability for SARS-CoV-2. *bioRxiv* (2021) doi:10.1101/2021.01.14.426475.
40. Chi, X. *et al.* A neutralizing human antibody binds to the N-terminal domain of the Spike protein of SARS-CoV-2. *Science (New York, N.y.)* **369**, 650 (2020).
41. Zhou, L. *et al.* Predicting spike protein NTD mutations of SARS-CoV-2 causing immune escape by molecular dynamics simulations. *chemRxiv* (2021) doi:10.33774/CHEMRXIV-2021-68ZN8.
42. Cov-Lineages. https://cov-lineages.org/global_report_P.1.html. *last visited 13-11-2021.*
43. Estimates of severity and transmissibility of novel SARS-CoV-2 variant 501Y.V2 in South Africa | CMMID Repository. https://cmmid.github.io/topics/covid19/sa-novel-variant.html. *last visited 13-11-2021.*
44. Funk, T. *et al.* Characteristics of SARS-CoV-2 variants of concern B.1.1.7, B.1.351 or P.1: data from seven EU/EEA countries, weeks 38/2020 to 10/2021. *Eurosurveillance* **26**, (2021).
45. Davies, N. G. *et al.* Increased mortality in community-tested cases of SARS-CoV-2 lineage B.1.1.7. *Nature 2021 593:7858* **593**, 270–274 (2021).
46. Muñoz-Fontela, C. *et al.* Animal models for COVID-19. *Nature 2020 586:7830* **586**, 509–515 (2020).
47. Bouwman, K. M. *et al.* Multimerization- And glycosylation-dependent receptor binding of SARS-CoV-2 spike proteins. *PLoS Pathogens* **17**, e1009282 (2021).
48. Richard, M. *et al.* SARS-CoV-2 is transmitted via contact and via the air between ferrets. *Nature Communications* **11**, 1–6 (2020).
49. Kim, Y. il *et al.* Infection and Rapid Transmission of SARS-CoV-2 in Ferrets. *Cell Host & Microbe* **27**, 704-709.e2 (2020).
50. Nagata, N. *et al.* Studies of Severe Acute Respiratory Syndrome Coronavirus Pathology in Human Cases and Animal Models. *Veterinary Pathology* **47**, 881–892 (2010).
51. Liang, L. *et al.* Pathology of Guinea Pigs Experimentally Infected with a Novel Reovirus and Coronavirus Isolated from SARS Patients. *DNA and cell biology* **24**, 485–490 (2005).
52. Brooke, G. N. & Prischi, F. Structural and functional modelling of SARS-CoV-2 entry in animal models. *Scientific Reports 2020 10:1* **10**, 1–11 (2020).
53. Chan, J. F.-W. *et al.* Simulation of the Clinical and Pathological Manifestations of Coronavirus Disease 2019 (COVID-19) in a Golden Syrian Hamster Model: Implications for Disease Pathogenesis and Transmissibility. *Clinical Infectious Diseases* **71**, 2428–2446 (2020).
54. Imai, M. *et al.* Syrian hamsters as a small animal model for SARS-CoV-2 infection and countermeasure development. *Proceedings of the National Academy of Sciences* **117**, 16587–16595 (2020).
55. Shi, J. *et al.* Susceptibility of ferrets, cats, dogs, and other domesticated animals to SARS–coronavirus 2. *Science (New York, N.y.)* **368**, 1016 (2020).
56. Schlottau, K. *et al.* Experimental Transmission Studies of SARS-CoV-2 in Fruit Bats, Ferrets, Pigs and Chickens. *SSRN Electronic Journal* (2020) doi:10.2139/SSRN.3578792.
57. Pickering, B. S. *et al.* Susceptibility of Domestic Swine to Experimental Infection with Severe Acute Respiratory Syndrome Coronavirus 2 - Volume 27, Number 1—January 2021 - Emerging Infectious Diseases journal - CDC. *Emerging Infectious Diseases* **27**, 104–112 (2021).
58. Vergara-Alert, J. *et al.* Piglets inoculated by different routes are not susceptible to SARS-CoV-2, but those inoculated parenterally were immunized against the virus. *Transboundary and Emerging Diseases* (2020) doi:10.1111/TBED.13861.
59. P, Z. *et al.* Fatal swine acute diarrhoea syndrome caused by an HKU2-related coronavirus of bat origin. *Nature* **556**, 255–259 (2018).
60. Chen, W. *et al.* SARS-associated Coronavirus Transmitted from Human to Pig. *Emerging Infectious Diseases* **11**, 446 (2005).
61. Harvey, W. T. *et al.* SARS-CoV-2 variants, spike mutations and immune escape. *Nature Reviews Microbiology 2021 19:7* **19**, 409–424 (2021).
62. de Haan, C. A. M. *et al.* Murine coronavirus with an extended host range uses heparan sulfate as an entry receptor. *Journal of virology* **79**, 14451–14456 (2005).
63. Laffeber, C. *et al.* Experimental Evidence for Enhanced Receptor Binding by Rapidly Spreading SARS-CoV-2 Variants. *Journal of Molecular Biology* **433**, 167058 (2021).
64. Qu, X. X. *et al.* Identification of two critical amino acid residues of the severe acute respiratory syndrome coronavirus spike protein for its variation in zoonotic tropism transition via a double substitution strategy. *Journal of Biological Chemistry* **280**, 29588–29595 (2005).
65. Sheahan, T. *et al.* Mechanisms of Zoonotic Severe Acute Respiratory Syndrome Coronavirus Host Range Expansion in Human Airway Epithelium. *Journal of Virology* **82**, 2274–2285 (2008).
66. Zech, F. *et al.* Spike mutation T403R allows bat coronavirus RaTG13 to use human ACE2 2. *bioRxiv* (2021) doi:10.1101/2021.05.31.446386.
67. Li, F. Structural Analysis of Major Species Barriers between Humans and Palm Civets for Severe Acute Respiratory Syndrome Coronavirus Infections. *Journal of Virology* **82**, 6984–6991 (2008).
68. Dinnon, K. H. *et al.* A mouse-adapted model of SARS-CoV-2 to test COVID-19 countermeasures. *Nature* **586**, 560–566 (2020).
69. Montagutelli, X. *et al.* The B1.351 and P.1 variants extend SARS-CoV-2 host range to mice. *bioRxiv* (2021) doi:10.1101/2021.03.18.436013.
70. Harcourt, J. *et al.* Severe Acute Respiratory Syndrome Coronavirus 2 from Patient with Coronavirus Disease, United States - Volume 26, Number 6—June 2020 - Emerging Infectious Diseases journal - CDC. *Emerging Infectious Diseases* **26**, 1266–1273 (2020).

71. Han, P. *et al.* Molecular insights into receptor binding of recent emerging SARS-CoV-2 variants. *Nature Communications 2021 12:1* **12**, 1–9 (2021).
72. Barton, M. I. *et al.* Effects of common mutations in the SARS-CoV-2 Spike RBD and its ligand, the human ACE2 receptor on binding affinity and kinetics. *eLife* **10**, (2021).
73. Thye, A. Y.-K. *et al.* Emerging SARS-CoV-2 Variants of Concern (VOCs): An Impending Global Crisis. *Biomedicines 2021, Vol. 9, Page 1303* **9**, 1303 (2021).
74. Kim, S. *et al.* Differential Interactions Between Human ACE2 and Spike RBD of SARS-CoV-2 Variants of Concern. *bioRxiv* (2021) doi:10.1101/2021.07.23.453598.
75. Chen, C. *et al.* Computational prediction of the effect of amino acid changes on the binding affinity between SARS-CoV-2 spike RBD and human ACE2. *Proceedings of the National Academy of Sciences* **118**, e2106480118 (2021).
76. Khan, A. *et al.* Higher infectivity of the SARS-CoV-2 new variants is associated with K417N/T, E484K and N501Y mutants: An insight from Structural data Observing VAT distribution and molecular changes with post-op management after metabolic surgery View project. *Article in Journal of Cellular Physiology* (2021) doi:10.1002/jcp.30367.
77. Baker, A. N. *et al.* The SARS-COV-2 Spike Protein Binds Sialic Acids and Enables Rapid Detection in a Lateral Flow Point of Care Diagnostic Device. *ACS Central Science* **6**, 2046–2052 (2020).
78. Bò, L. *et al*. Exploring the Association Between Sialic Acid and SARS-CoV-2 Spike Protein Through a Molecular Dynamics-Based Approach. *Frontiers in Medical Technology* **0**, 24 (2021).
79. Connor, R. J. *et al.* Receptor Specificity in Human, Avian, and Equine H2 and H3 Influenza Virus Isolates. *Virology* **205**, 17–23 (1994).
80. Childs, R. A. *et al.* Receptor-binding specificity of pandemic influenza A (H1N1) 2009 virus determined by carbohydrate microarray. *Nature Biotechnology 2009 27:9* **27**, 797–799 (2009).
81. Lam, S. D. *et al.* Insertions in the SARS-CoV-2 Spike N-Terminal Domain May Aid COVID-19 Transmission. *bioRxiv* (2021) doi:10.1101/2021.12.06.471394.
82. Yao, W. *et al.* Circulating SARS-CoV-2 variants B.1.1.7, 501Y.V2, and P.1 have gained ability to utilize rat and mouse Ace2 and altered in vitro sensitivity to neutralizing antibodies and ACE2-Ig. *bioRxiv* (2021) doi:10.1101/2021.01.27.428353.

Supplementary figures

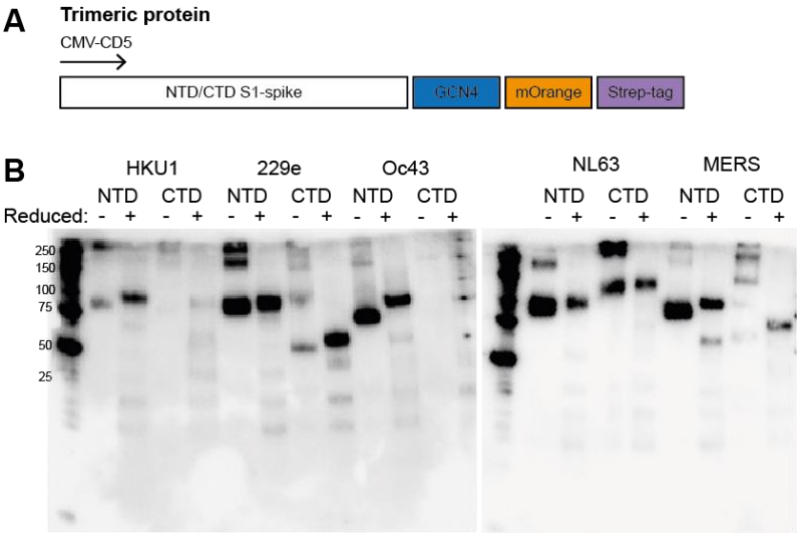

Supplementary figure 1: Western blot of purified HCoV-NTDs and CTDs. A Schematic overview of used expression vector. **B** Western blot of purified trimeric NTDs and CTDs of the HCoVs. For each protein, an equal concentration of protein was loaded onto the gel.

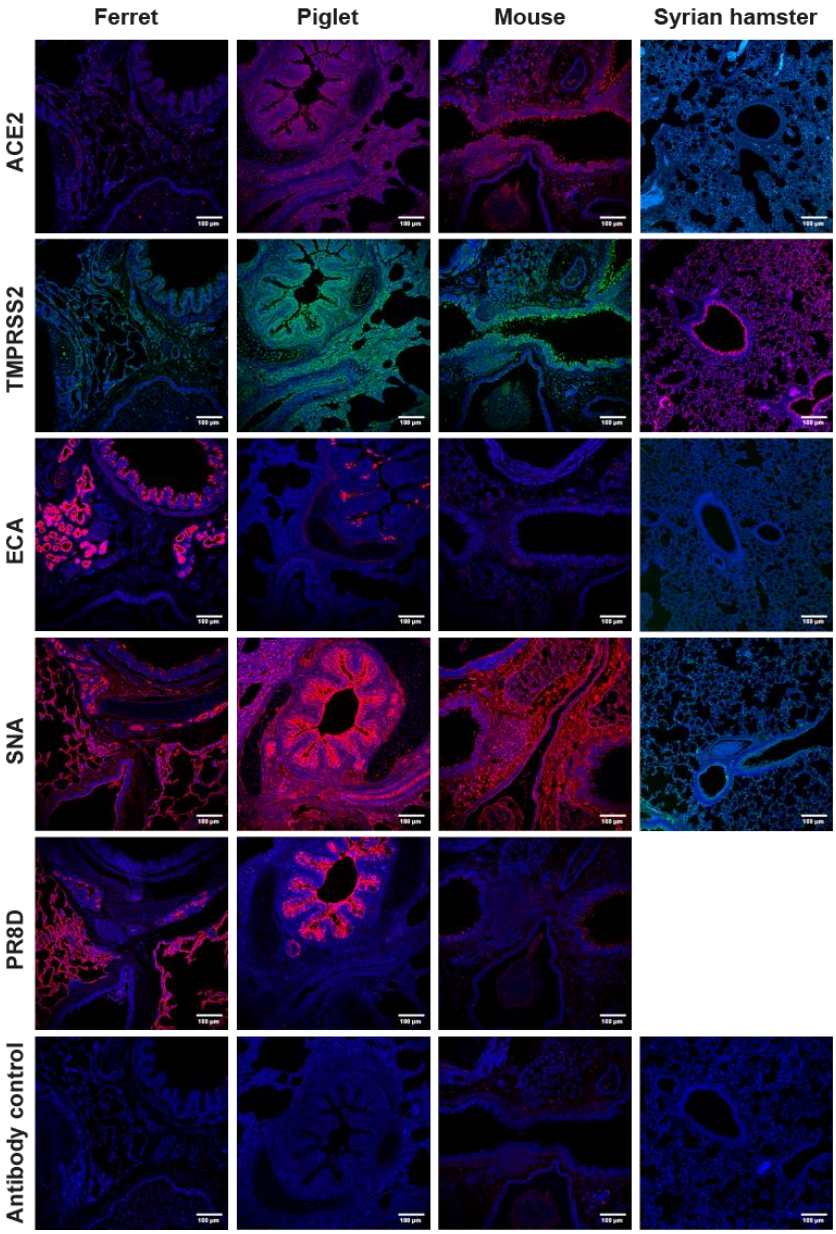

Supplementary figure 2: Validation of used lung tissues. Most lung tissues that were used for the experiments were stained with ACE2-ab, TMPRSS2-ab, ECA and SNA to confirm the presence of ACE2, TMPRSS2, galactose, terminal glycans and 2,6-linked sialic acids respectively. Also, stainings with PR8D, that is known to bind some 2,6-linked sialic acids and an antibody control were performed. ACE2-ab, TMPRSS2, SNA and ECA were applied at 5 µg/ml and PR8D at 50 µg/ml.

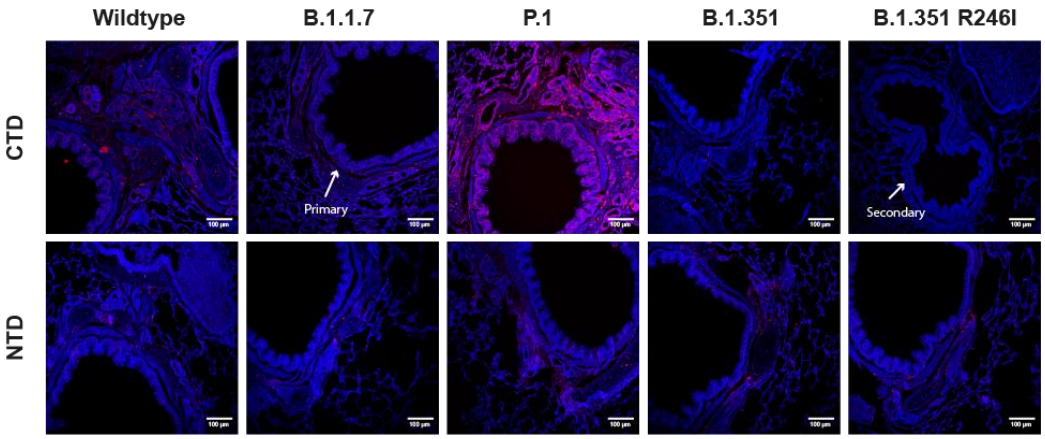

Supplementary figure 3: Ferret primary and secondary bronchiolar structures. Ferret lung tissues were stained with NTD and CTD S1-spike proteins of the VOCs. Here, primary and secondary bronchiolar structures are displayed and appointed with arrowheads. Proteins were applied at 50 µg/ml.